The hunt for elusive molecules: Insights from joint theoretical and experimental investigations

Marie-Aline Martin-Drumel[*], Joshua H. Baraban[†], P. Bryan Changala[‡], John F. Stanton[§], Michael C. McCarthy[¶]

Mini-review

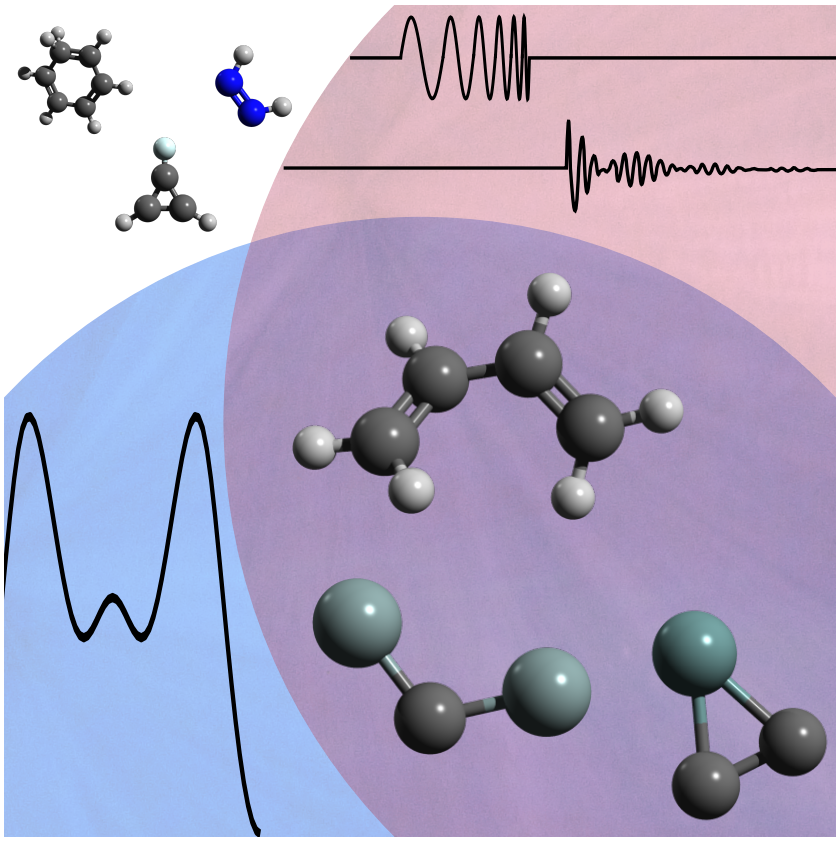

[*]Institut des Sciences Moléculaires d'Orsay (ISMO), CNRS, Univ. Paris-Sud, Université Paris-Saclay, F-91405 Orsay (France)

[†]Department of Chemistry, Ben-Gurion University of the Negev, Beer-Sheva 8410501, Israel

[‡]JILA, National Institute of Standards and Technology and Department of Physics, University of Colorado, Boulder, CO 80309, United States

[§]Quantum Theory Project, Depts. of Chemistry and Physics, Univ. of Florida, Gainesville, FL 32611, United States

[¶]Harvard-Smithsonian Center for Astrophysics, Cambridge, Massachusetts 02138, United States

Abstract:

Rotational spectroscopy is an invaluable tool to unambiguously determine the molecular structure of a species, and sometimes even to establish its very existence. This article illustrates how experimental and theoretical state-of-the-art tools can be used in tandem to investigate the rotational structure of molecules, with particular emphasis on those that have long remained elusive. The examples of three emblematic species — *gauche*-butadiene, disilicon carbide, and germanium dicarbide— highlight the close, mutually beneficial interaction between high-level theoretical calculations and sensitive microwave measurements. Prospects to detect still other elusive molecules of chemical and astronomical interest are discussed.

Keywords: Rotational spectroscopy, Ab initio calculations, Structure elucidation

1 Introduction

Rotationally-resolved spectroscopy has proven to be an extremely powerful tool for unambiguously identifying new chemical species and determining their molecular structures. Because every molecule has a unique three-dimensional structure, it also possesses a characteristic set of rotational constants that are inversely proportional to its moments of inertia. At high spectral resolution, even very similar compounds such as isomers, conformers, or isotopologues of molecules and weakly bound intermolecular clusters can be readily distinguished on this basis (e.g., Refs.[1,2] and references therein).

Pure rotational spectroscopy has been employed with great effectiveness to identify a wide range of compounds in the gas phase; these discoveries are not limited solely to the laboratory but extend to the terrestrial atmosphere and the interstellar medium as well. Nearly 90 % of the more than 200 known astronomical molecules, for example, have been observed via their pure rotational spectrum.[3,4] Although many types of compounds including both stable and transient species (e.g., high-energy isomers, radicals, ions, etc.), and some of considerable size and complexity, have been successfully characterized by these methods, a surprising number of fundamental species have evaded direct experimental characterization, including some that naively appear simple. These so-called "elusive" molecules are in fact key intermediates in reaction pathways by which more complex molecules are thought to form. In some cases their very existence has been a topic of considerable debate, and in nearly all cases questions surround their molecular structure. For these reasons, there is great practical value in isolating and spectroscopically characterizing these "elusive" molecules. By doing so

chemical models with improved predictive power can be developed, the abundance of these species in chemical reactions can be quantified, and searches in celestial objects by remote sensing become feasible.

What makes a species elusive? And how have some small but fundamental species resisted direct detection or defied meaningful structural characterization for so long? This "elusive" classification is of course subjective, since the process by which the pure rotational spectrum of any new species is detected in the laboratory is often non-trivial and many practical factors come into play, from the accuracy of the predictions, the experimental conditions, to the method of spectral assignment. For example, predicted rotational frequencies based on theoretical calculations of the molecular structure of elusive species may be highly uncertain and thus often require searches over a wide spectral range. Additionally, transitions may also be quite weak if the permanent electric dipole moment is small. Consequently experimental searches can be extremely time consuming. Furthermore, reactive species can rarely be synthesized selectively, and instead are produced by methods such as electrical discharge, photolysis, laser ablation, etc. that produce a wide range of species. Generating such species in high steady-state abundance may be very difficult because they often react at or near the gas-kinetic rate with many other species that are simultaneously produced. Finally, the assignment of large numbers of molecular transitions is tedious when many molecules are produced simultaneously.[5]

Although elusive molecules usually fall into one or more of the above categories, the most common challenge is the detection of species with small calculated dipole moments and/or low steady-state abundances, which is compounded by the ever-present uncertainty as to

the frequencies of their rotational transitions. Accordingly, laboratory identification is often aided enormously by predictions obtained from high-level quantum chemical calculations. In particular, while the rotational spectrum of a molecule can be described to zeroth-order by only three rotational constants* (A, B, C), it can be difficult to predict at a level of accuracy that approaches the extreme resolution typical of rotational spectroscopy. Furthermore, many other parameters may be needed to adequately describe a rotational spectrum at high resolution: centrifugal distortion for non-rigid molecules, hyperfine constants for atoms with non-zero nuclear spins, spin-orbit constants for open-shell species, Coriolis interactions, tunneling splittings, and a virtually limitless pantheon of possible perturbations. For all of these reasons, the combination of very accurate theoretical calculations and extremely sensitive pure rotational measurements is ideally suited to observe and characterize elusive species.

In the last 10 years, we have successfully exploited the close coordination of theoretical calculations and rotational spectroscopy to detect and structurally characterize several elusive species. In this review, we describe three emblematic species whose experimental observations were only made possible by this close interaction: *gauche*-butadiene,[6] SiCSi,[7] and GeC_2.[8] Prospects to detect other elusive species are also discussed.

*While three rotational constants are generally required to describe a molecule, fewer constants can be needed in some specific cases; for example, strictly linear chains require a single constant B.

2 Experimental and computational tools

2.1 Fourier-transform microwave spectroscopy

A key advantage of studying molecules in the microwave or centimeter domain (i.e., roughly 1–50 GHz) is that rotational transitions between low-J energy levels are sampled. These levels are in many respects "pristine", i.e., only rarely affected by perturbations that more commonly affect non-rigid molecules or by centrifugal distortion which usually scales as powers of J or other quantum numbers. As a result, a rigid rotor model with at most three rotational constants (A, B, C) is usually sufficient to reproduce rotational spectra in this region (in the absence of fine or hyperfine structure). The spectroscopic analysis is thus generally straightforward, and the experimentally-derived constants can be readily compared to theoretical predictions. Over the last 40 years, Fourier-transform microwave (FTMW) spectroscopy has emerged as a powerful spectroscopic tool in the discovery and investigation of gas-phase species. This time-domain technique involves polarizing a gas sample with an intense pulse of microwave radiation. Provided the frequency of one or more rotational transitions falls within the bandwidth of the excitation pulse, a coherent macroscopic polarization results. Since the coherence lifetime is normally long compared to either the excitation pulse (of the order of 1 µs) or the ringdown time of the resonator from the purely instrumental effects, this polarization is then detected in an essentially background-free environment using a microwave receiver shortly after the excitation pulse (within a few µs). The Fourier-transform of this time domain signal then yields a spectrum in the frequency domain with a bandwidth commensurate with the length of the excitation pulse.

Traditional FTMW spectroscopy combines monochromatic microwave radiation and a high-Q Fabry-Pérot cavity to greatly increase the effective path length. Developed in the mid 1980's by Flygare and co-workers,[9] sufficient microwave power is normally available in this variant to achieve the $\pi/2$ condition for molecules with dipole moments as low as 0.1 D, or sometimes even smaller.[10] Beyond sensitivity, a key aspect of cavity-enhanced FTMW spectroscopy is that line intensities scale linearly with the dipole moment μ, and not with μ^2 as in conventional absorption rotational spectroscopy.[11] As a consequence, rotational lines of weakly polar molecules are more readily detected by this method compared to either classical emission or absorption spectroscopy. Detection sensitivity is achieved at the expense of instantaneous bandwidth (IB), however, which is limited to about 1 MHz (assuming a pulse length of $\sim$1 µs), making spectral surveys over hundreds of MHz extremely tedious by manual operation. This purely technical limitation, however, has been largely overcome in recent years with custom control and analysis software developed by several groups.[5,12–14]

Driven by the commercial availability of both arbitrary waveform generators capable of generating GHz-wide frequency chirps and high-speed digital oscilloscopes with sampling rates of many tens of GSa/s, a second variant of FTMW spectroscopy, commonly referred to as chirped-pulse (CP) or broadband FTMW, was developed a decade ago by Pate and colleagues.[15] In this variant, a linear frequency chirp is amplified, alone or after mixing with a local oscillator, in real-time with a high-power traveling wave tube amplifier (TWTA). Following passage through the absorbing gas, the coherent macroscopic sample is detected with a microwave receiver, and directly digitized on the high-speed oscilloscope in real time. By doing so, spectra over many GHz can be routinely recorded for each gas pulse. In

combination with a flat instrumental response function, it is then often possible to convert line intensities to abundances,[16,17] which in turn enables one to comprehensively quantify the gas composition for a given set of experiment conditions. Because of the difficulty of achieving the $\pi/2$ pulse condition for weakly polar molecules in this arrangement, line intensities often scale as μ^2,[15] making low dipole moment species more challenging to detect (but still often feasible) compared to the cavity-enhanced FTMW variant.

A third variant of FTMW spectroscopy, intermediate between the narrow band, cavity-enhanced and extremely wide IB versions, has received considerable attention in the past five years. In this variant, relatively small frequency segments ($\sim 200\,\mathrm{MHz}$) are instead acquired in a manner similar to the broadband version, by mixing a low-frequency linear chirp with a local oscillator at a fixed frequency.[18,19] By synchronously switching the local oscillator frequency, many individual segments can be automatically and seamlessly stitched together under computer control. An important practical advantage of segmented FTMW instruments is cost, since the sampling rate and bandwidth requirements of the arbitrary waveform generator and digital oscilloscope are greatly reduced, and relatively inexpensive solid state amplifiers can be used instead of higher power TWTAs. Table 1 compares several key aspects of the three widely used FTMW techniques. It should be noted that since these types of spectrometers are generally not commercially available, ones with other characteristics have also been reported. These include cavity-enhanced versions that operate at the lower end of the millimeter-wave band;[20,21] both waveguide[22–24] and free-space instruments[25,26] that operate throughout the radio band, which are often, but not exclusively, used in combination with a static gas sample at or near room temperature and low pressure; and in-phase/quadrature-

phase-modulation passage-acquired-coherence techniques (IMPACT[27]), to highlight a few.

2.2 Sample preparation and rotational cooling

Two key requirements are needed to investigate the pure rotational spectrum of a molecule in the microwave domain: i) some fraction of the molecular sample must be present in the gas phase; and ii) this gas-phase component has to be rotationally cold enough so that its lower rotational energy levels are populated. Both requirements can be achieved by one of two approaches: adiabatic (i.e., supersonic) expansion or buffer gas cooling. A side-by-side comparison of their strengths and weaknesses is summarized in Table 2.

Adiabatic expansion sources have been widely used since the late 1970s to rotationally cool molecules for subsequent spectroscopic study.[28] With respect to FTMW spectroscopy specifically, this type of source greatly improves the detection sensitivity because the rotational temperature ($T_{rot} = 2 - 10\,K$) of the sample and the nominal frequency range ($\leq 40\,GHz$) of the microwave spectrometer are well coupled. Rotational cooling is typically achieved by pulsing the sample of interest, heavily diluted in a buffer gas (usually Ar or Ne), into a vacuum chamber via a pinhole orifice (much like a fuel injector); typically the length of each gas pulse is about 1 ms or less, and the duty cycle is very low (see Table 2). The sample of interest might be either a gas or have significant vapor pressure, or it might be volatilized by heating, e.g., thermally or by laser ablation. Regardless, owing to the very large pressure differential behind the nozzle (0.5-5 atm) versus that in the vacuum chamber (of order 10^5–10^8), supersonic expansion of the gas takes place within a few nozzle diameters of the

orifice, and the rotational temperatures rapidly drops as the gas reaches terminal velocity. Rotational temperatures in the 2–10 K vicinity are routinely achieved, even though the vibrational and electronic degrees of freedom are rarely cooled to the same extent. Although both commercial (e.g., General Valve Series 9) and custom valves (e.g., Even Lavie) can operate at high repetition rates, much lower rates are common for rotational experiments, often a few tens of Hz or slower, even when high-speed vacuum pumps are used. This low rate is set by two factors: i) the large amount of buffer gas (typically present at the level of 99 %) that is required to achieve efficient rotational cooling during each gas pulse, and ii) the sensitivity of the free induction decay to collisional dephasing, which sets a stringent requirement for the base pressure in the chamber.

Transient species are most commonly produced either by applying a high voltage potential (typically 1 kV) between two electrodes in the throat of the nozzle, or by ablating a solid rod of the desired precursor by striking it with a tightly focused laser pulse. In this latter configuration, the rod is positioned just after the nozzle orifice, and the timing of the laser pulse is synchronized with the opening of the nozzle orifice so as to entrain the ablated products in the gas expansion. In some instances, the combination of laser ablation and an electrical discharge has been used with good success to detect small metal-bearing species that are not efficiently produced by either laser ablation or an electrical discharge alone.[29]

A second cooling approach, cryogenic buffer gas cooling, has been exploited for spectroscopic investigation of large molecules in recent years.[30,31] Although originally developed by De Lucia and co-workers as a method to study collisional broadening of astronomical species at the very low temperatures characteristic of interstellar clouds,[32] renewed inter-

est in this cooling method stems from its promise to gently but uniformly cool molecules in nearly all internal degrees of freedom, an essential requirement in many atomic, molecular, and optical physics applications, including quantum control[33]. Buffer gas cooling has been used in combination with laser-ablation to generate cold diatomics,[34,35] to detect Rydberg–Rydberg transitions in the millimeter band,[36] in laser-induced fluorescence spectroscopy,[30,37] to detect enantiomers[38,39] and their state-specific transfer by rotational spectroscopy,[40] in infrared frequency comb studies[31,41], and in time-domain studies of conformational relaxation.[42]

This cooling scheme has several important attributes: very high repetition rates can be achieved, small quantities of sample are needed, the system temperature is an order of magnitude lower than that of cavity-enhanced FTMW spectrometers, and chemistry and cooling can be controlled separately. Because the timescale required to rotationally cool the sample to 10 K or less with cold He atoms is short compared to the diffusion time of the sample to the cell walls, the sample can be interrogated repeatedly. Since a continuous refrigerant is available, small quantities of pure samples can be continuously injected into the cell which implies that repetition rates, no longer limited by the nozzle operation and pumping efficiency, are in the range of several tens of kHz (i.e. 35 kHz, due to other purely instrumental limitations), in sharp contrast to the very low duty cycle characteristic of supersonic nozzle. Because the cell is cryogenically cooled, it is also possible to use very low noise receivers (about 1 K/GHz) and protection switches, and thereby achieve a system temperature (20–40 K) close to the fundamental limit set by modern technology (owing to the large dimensions of open-resonators, the system temperature of cavity-enhanced FTMW spectrometers is at least an

order of magnitude higher, even when the Fabry-Pérot mirrors and first-stage amplifier are cooled to liquid nitrogen temperatures[14]). Finally, in principle, chemistry and cooling can be independently adjusted and controlled because cooling is separate from the sample source.

Heat loading is arguably the most severe limitation in buffer gas experiments. Because the cooling capacity of the system is quite low ($\sim$ 1 W), the gas load must be carefully controlled. Since pumping of He and molecular input is achieved with a cryogenic activated charcoal adsorbent ("sorb"), as opposed to a mechanical pump, thermal cycling of the system is required upon sorb saturation (roughly every 20 hours of run-time), i.e. the system must be warmed to room temperature and then cooled down again. This cycle time is significant, usually of order 1–2 days, in contrast to an experiment using a supersonic expansion where continuous operation for long periods of time is common, and downtime to service the nozzle source is normally performed in a matter of minutes. Experiments involving an external excitation source to produce transient species, such as a discharge or pyrolysis experiment, require careful engineering to allow dissipation of excess heat.[43] Nevertheless, an intriguing aspect of buffer gas cells is the ease with which solid[44] and neat liquid samples can be used — the latter are readily volatilized by direct injection into the cell — making this technique very attractive for characterization of chemical compounds produced from chemical synthesis.

2.3 Experimental set-ups

In the microwave investigations of the elusive species described here, different cooling methods and variants of FTMW spectroscopy have been used: cavity-enhanced FTMW spectroscopy

in combination with a supersonic expansion and CP-FTMW spectroscopy using either a supersonic expansion or a buffer gas cell (Figure 2). Additional details of each experimental combination follow.

Cavity-enhanced FTMW spectroscopy with a supersonic expansion Our cavity-enhanced FTMW instrument operates between 5 and 40 GHz, and has a similar design and dimensions to the original Balle-Flygare spectrometer.[9] Many experimental details have been given elsewhere[45] so only a brief summary of this instrument is provided here. Owing to the sensitivity advantage of co-aligning the supersonic expansion with the axis of the cavity[46] the gas sample is routinely injected in the vacuum chamber via a small hole in one of two cavity mirrors. With this geometric arrangement each rotational line is split by the Doppler effect into a well-resolved doublet (Figure 2), in which the rest frequency of the transition is derived by simply averaging the frequencies of two symmetrically-displaced components. Since the transit time of the gas through the beam waist of the cavity is relatively long in this arrangement, linewidths are quite sharp, about 5 kHz full-width at half maximum (FWHM), yielding line frequencies that are accurate to 1–2 kHz for non-magnetic species; owing to the effect of residual magnetic fields, Zeeman broadening may reduce the frequency accuracy of the lowest-J lines of some open-shell radicals to 5–10 kHz. Powerful in-house acquisition software enables efficient tuning of the cavity (i.e., displacement of the moving mirror) throughout the entire frequency range of the spectrometer, so that wide frequency surveys can be performed in a fully automated fashion.[5]

CP-FTMW spectroscopy with a supersonic expansion Our CP-FTMW spectrometer closely follows the design of Pate and co-workers,[15] and covers the 2–26 GHz region in three bands: 2–8, 8–18, and 18–26 GHz (the highest frequency band is under its final steps of development). Since this CP-FTMW spectrometer is located in the same vacuum chamber as the cavity-enhanced FTMW instrument, but lies on a perpendicular axis, the same supersonic expansion is used with both experimental set-ups, and it is straightforward to quickly switch between the two. This CP-FTMW spectrometer and its in-house acquisition software have been described in a recent publication[5]. Typical Fourier-transformed limited linewidths using our instrument are about 100 kHz FWHM, thus the frequency accuracy is on the order of 10–50 kHz, depending on the SNR.

CP-FTMW spectroscopy in a buffer gas cell The third experimental combination used in our laboratory involves CP-FTMW spectroscopy and buffer gas cooling (Figure 2). In this arrangement,[6,44,47] a small buffer gas cell (roughly 10 cm on each side), cooled to 4–7 K with the second stage of a two-stage closed cycle He cryostat, resides inside an outer jacket that is held at 70 K, which is in turn thermally isolated from the room temperature walls of the vacuum chamber. Helium gas enters the buffer gas cell via a pre-cooled line (4 K) at a typical flow rate of 5–10 sccm, which results in a density of approximately 10^{14} He atoms/cm^3 in the cell. Another aperture allows for sample input through a small hole on one face of the cell; for gas samples, a heated stainless steel capillary is used and the flow of gas is normally controlled with a mass flow controller (1–10 sccm). Because molecules collisionally thermalize in nearly all internal degrees of freedom within roughly 100 collisions, and because collisions occur once every 10–20 µs, molecules reach equilibrium with the cold

He gas in about 1 ms. The diffusion time to the cell walls, however, is an order of magnitude longer (15–20 ms), meaning there is a relatively long observation time prior to freezing out on the cell walls.

Molecules are excited and detected using a pair of matched microwave horns, one set operating between 12 and 18 GHz, and the other between 18 and 26 GHz. By using a spherical mirror and positioning both horns on the same side of the cell, it is possible to increase the path length by a factor of two. Broadband spectra are acquired by concatenating together relatively narrow frequency segments, each with a bandwidth of 100–250 MHz. Owing to the lifetime of molecules in the cell, the repetition rate of the microwave circuitry is high, typically in the 25–35 kHz range. Because the local oscillator and data acquisition is computer controlled, it is possible to rapidly cover the full band (either 6 or 8 GHz) of each circuit.

2.4 Computational methods

Computing a high accuracy rotational spectrum of a molecule typically involves combining several quantum chemistry calculations. The theoretical methods that have assisted the work described in this paper are those which are able to predict various spectroscopic parameters (rotational and centrifugal distortion constants, vibration-rotation interaction, tunneling splittings, etc.) at a level of accuracy sufficient to significantly facilitate experimental searches, and to convincingly confirm or reject experimental assignments. At the simplest level, predictions of the rotational constants require an accurate molecular structure; the centrifugal distortion constants require a harmonic force field, and rotation-vibration constants

additionally require the cubic force field (third derivatives of the potential energy surface). More complex calculations of quantities such as the tunneling splitting (a vital part of the butadiene work described later) require accurate and relatively elaborate characterization of the potential energy surface over fairly large domains of nuclear displacement. Moreover, the simplest treatment of vibrational effects on rotational constants — which is that based on second-order vibrational perturbation theory (VPT2)[48] — can be inadequate, and calculations that require more flexible coordinate systems and more extensive information about the potential energy surface may be needed.

The foundation of all these theoretical calculations is an accurate potential energy surface, which requires accurate solutions to the electronic Schrödinger equation. The method of choice for applications to spectroscopy is single-reference coupled-cluster (CC) theory,[49] especially when the relevant nuclear motions are largely limited to regions near the equilibrium geometry. In general, quite accurate equilibrium structures can be obtained by treating the electron correlation using the CC method with iterative inclusion of single and double excitations and perturbative inclusion of triple excitations [CCSD(T)][50] in conjunction with large basis sets. Combining the equilibrium rotational constants (B_e) obtained from these structures with vibrational corrections computed at somewhat more economical levels of theory generally gives ground-state rotational constants (B_0) that are comfortably within 1% of experiment, which significantly facilitates laboratory searches for molecules present in the complex mixtures often produced by electrical discharges. In general, the CCSD(T) method is the approach used to treat the effects of electron correlation, and basis sets used to determine the equilibrium geometry (ideally by extrapolation) are the core-correlating

correlation consistent sets, cc-pCVXZ. These exist at the double, triple, quadruple, and pentuple "zeta level", where X=D, T, Q, and 5, respectively, and their use is important because they properly describe correlation effects involving core electrons. While "core correlation" is often ignored in the calculation of thermodynamic energy differences (and spectroscopic energy differences, which are not unrelated), it does impact molecular structure and must be considered when striving for the level of accuracy that we seek in aiding our experimental efforts. In passing, it should be noted that accurate and economical results for equilibrium geometries are often obtained merely with the cc-pCVQZ basis when using CCSD(T). While the larger (and more expensive) cc-pCV5Z basis is more complete and therefore "better", it transpires that the residual effects of basis set expansion beyond a certain level are to shorten bond lengths. This tends to cancel with the effects of residual electron correlation effects beyond CCSD(T), which characteristically lengthens bond distances.[51] Such higher-order correlation effects are typically accounted for by adding a CCSDT(Q) correction calculated with a small basis set, and can be decidedly non-negligible. Finally, electronic contributions to the moments of inertia can also be significant,[52] and obviously special circumstances, such as the need for augmented basis sets, may dictate changes to the recipe for success.[49]

One type of special circumstance would be when molecular size mitigates against the application of such accurate – and expensive – quantum-chemical methodology. While our work in the past based on the high-level CCSD(T)/cc-pCVXZ treatments has been restricted to molecules with roughly a half-dozen non-hydrogen atoms (phenyl being such an example[53,54]), it is worthwhile to briefly touch on what might be done for larger systems (with, say, a dozen non-hydrogen atoms). Here, the technique of density functional theory (DFT) is

widely used, and of course the relevant quantities (equilibrium geometries, rotation-vibration constants, etc) can be computed with DFT. However, the accuracy achievable in such an approach does not rival that of the more expensive (and theoretically robust) approach that we use in our studies, and the prediction of rotational constants is less satisfactory. However, for studies of larger molecules, it remains a viable and popular approach.

While effects of the easily-calculated centrifugal distortion constants are almost negligible for the ground state rotational constants, effects of vibrational-rotation interaction are important, and often under-appreciated, as their magnitude is sufficiently large to be comparable to, and often exceed, the overall uncertainty in the final prediction of the ground state rotational constants. Moreover, the values of the individual constants are needed to estimate and to help assign transitions in vibrationally excited states. While vibrational perturbation theory provides reasonable values for many molecules, when high accuracy is required, or in unusual molecules, it is essential to perform a more advanced treatment. Basic calculations of the rotation-vibration constants typically done in our work use VPT2[48] and the CCSD(T) method, but generally are done in the frozen-core approximation with basis sets appropriate to such calculations. Previous work has shown that the atomic natural orbital sets known as ANOX (X=0, 1 and 2 are double, triple and quadruple "zeta" quality) give a good representation of the anharmonic force field (through quartic constants) as inferred by the corresponding predictions of fundamental vibrational frequencies by VPT2.[55] Since the force constants that play a role in the vibration-rotation constants are a subset of those needed to compute fundamental frequencies, they should provide values of α_i^B comparable in accuracy to vibrational frequencies.

Occasionally, however, VPT2 is inadequate. This generally is the case for large amplitude motion, and is always the case when more than one dynamically accessible minimum exists on a potential energy surface. For small molecules with fewer than four or five atoms, numerically exact variational nuclear motion calculations yield high accuracy rovibrational energies and spectroscopic constants limited only by the underlying potential energy surface.[56] One example of such a calculation from our work below is the floppy SiCSi molecule. For larger non-rigid molecules, however, direct variational calculations are computationally prohibitive. A typical example here is *gauche*-butadiene, a chiral molecule in which the R and S enantiomers are separated by a potential energy barrier of less than 200 cm^{-1}. Non-rigid, multiwell systems such as this have recently motivated the development of a rovibrational method based on curvilinear second-order vibrational Møller-Plesset perturbation theory (VMP2).[57] Curvilinear VMP2 improves upon standard VPT2 in two key respects: i) the harmonic zeroth order wavefunction of VPT2 is replaced with an anharmonic zeroth order wavefunction, comprising a variationally optimized product of one-dimensional wavefunctions for each vibrational coordinate; and ii) the standard rectilinear vibrational normal coordinates used in VPT2 are replaced with arbitrary curvilinear internal coordinates. The curvilinear coordinates are chosen to increase the separability of the vibrational Hamiltonian, thereby significantly improving the accuracy of the zeroth order product wavefunction. The "correct" choice is dictated by the underlying dynamics of the molecule. For example, for isomerizing systems like *gauche*-butadiene we use a curvilinear reaction path coordinate system that naturally interpolates between the two enantiomer wells. This relatively sophisticated zeroth order picture forms the basis for second-order perturbation theory, which yields anharmonic vibrational frequencies, tunneling splittings, rotational and centrifugal distortion

constants, and rotation-vibration interaction parameters.[58]

2.5 Semi-experimental equilibrium structures

Once a complete laboratory assignment of the rotational spectrum is available, a precise semi-experimental equilibrium structure of the species (r_e^{SE}) can be derived. To do so, however, three requirements must be fulfilled: i) a partial or complete set of experimental rotational constants should be determined for as many isotopic species as possible; (ii) the number of experimental rotational constants must at least meet, and ideally exceed, the number of free structural parameters (bond lengths, bond angles, dihedral angles); and (iii) vibrational contributions must be removed from these rotational constants to yield semi-experimental equilibrium rotational constants (A_e^{SE}, B_e^{SE}, and C_e^{SE}).

The first two requirements are usually achieved by performing extensive isotopic measurements either in natural abundance or with an isotopically-enriched sample, under the assumption that isotopic substitution has no effect on the geometrical structure. When the number of possible isotopic substitution is limited (low natural abundance, limited availability of an enriched precursor), the number of experimental rotational constants may not allow a full structure determination. In this instance some of the geometrical parameters are normally frozen to their theoretical values, and only a partial experimental structure is derived.

The third requirement again highlights the close coordination between experiment and theory. While vibrational effects can in principle be determined entirely by experimental

means, it requires knowledge of all vibration-rotation constants, α_i^B (i.e. for all three rotational constants) in all vibrational modes. While this is routinely done for diatomics and regularly on polyatomics with three to four atoms, examples of purely experimentally determined equilibrium structures for larger species are rather sparse.[59] Since the number of vibrational modes ($3N-6$ for a non-linear molecule) increases very rapidly with the number of atoms (N) in the molecule; high-lying vibrational states may be poorly or unevenly populated, and thus hard to probe in absorption by rotational spectroscopy. Furthermore rotationally-resolved vibrational spectroscopy may be difficult, even at the highest resolution available for infrared and far-infrared spectroscopy, and consequently the experimental determination of complete sets of α_i^B quickly becomes prohibitive for large species. When no information on α_i^B is available, an r_0 experimental structure can be derived instead using the available rotational constants in the vibrational ground state. It is, however, standard practice to determine a r_e^{SE} structure[60] by correcting the ground state rotational constants using the calculated vibrational constants (Figure 3) to yield semi-experimental equilibrium rotational constants. Such semi-experimental structures can then be compared directly to those calculated purely by theory and to those obtained for related molecules by similar means with little ambiguity.

In summary, the interplay between experiment and theory is central to the investigation of elusive species. High level calculations are the foundation that guide sensitive experimental searches, but input from experimental observations and measurements is critical in practice for designing the best possible theoretical treatments. In return, accurate experimental rotational constants are the basis for determining highly accurate structures of the formerly

elusive species of interest (Figure 3).

3 Examples of characterized elusive species

3.1 *gauche*-butadiene

Butadiene, C_4H_6, the simplest diene, is a relatively well-known molecule, at least in its most stable *trans* form where it has been characterized intensively in the gas phase (see e.g., Ref.[61]). Until recently though, relatively little was known about its second stable form, *cis* or *gauche*, even though this conformer is the archetypal species for the Diels-Alder reaction, one of the most commonly used and studied mechanisms in organic chemistry (Figure 1). This minor conformer is calculated to lie in a substantial minimum on the potential energy surface and to have a non-negligible abundance relative to the *trans* conformer at room temperature (about 2 %) because it lies only ∼15 kJ/mol higher in energy. Despite these favorable factors, it has long avoided direct experimental observation and its structure, planar or not, was itself a matter of debate.[62] Early calculations predicted a planar *cis* form, owing to double-bond conjugation which should impart a strictly two dimensional geometry, but with the advent of accurate quantum chemical methods, consensus was reached on a non-planar, *gauche* form presumably owing to the importance of a competing effect — steric interaction of the two terminal inner hydrogens. Nevertheless, the extent of the out-of-plane angle remained uncertain (e.g., Ref.[63]). Unlike the centrosymmetric *trans* form that has no permanent dipole moment, the *gauche* form is very weakly polar, with a calculated permanent dipole

moment on the order of 0.1 D. This vanishingly small value makes it nearly impossible to detect by conventional absorption spectroscopy, but a viable, although challenging, candidate for FTMW spectroscopy.

Both high-level calculations and FTMW measurements have enabled the first rotationally resolved characterization of this conformer.[6] First, accurate calculations were performed at AE-CCSD(T)/PCVQZ (r_e) + FC-(T)/CCSD(T)/ANO0 VPT2 (α) level of theory to provide preliminary rotational constants (Table 3). Using these constants as a guide, experimental investigations were undertaken using CP-FTMW spectroscopy in a buffer gas cell using cryogenic helium. Gaseous butadiene was injected through a warm capillary ($T = 230\,^{\circ}\mathrm{C}$) to increase the *gauche*/*trans* ratio. Very soon afterwards, two transitions were observed within 0.1 % of the prediction for the $1_{1\,0} - 1_{0\,1}$ transition (Figure 5). These experimental lines, and additional ones that we subsequently measured, appear as doublets of comparable intensity, prompting us to delve deeper in the calculations on the assumption that this line structure arises from tunneling splitting between the two equivalent *gauche* forms (Figure 4). Eventually, calculations using curvilinear second order rovibrational Møller–Plesset perturbation theory[57] on a full dimensional potential surface reproduced the tunneling effects very accurately, leading to ultimate theoretical rotational constants (including a refined equilibrium structure) that were within 6 MHz of experiment for all isotopologues (Table 3). Intriguingly, the unexpectedly fast tunneling time of tens of ps explains perfectly the apparent planar C_{2v} structure observed previously in matrix infrared experiments.[64–67]

Once the first rotational lines of *gauche*-butadiene were detected, subsequent measurements were performed using the cavity-enhanced FTMW instrument. Interestingly, while

the 0^+ and 0^- transitions were of roughly equal intensities in the buffer gas cell experiment, the 0^- lines were at least 10 times weaker in the cavity instrument, a likely reflection of the different cooling mechanisms at play. If the tunneling motion had not been revealed by the initial CP-FTMW experiment in the buffer gas cell, the 0^- transitions would most likely have avoided experimental detection on the basis of cavity-enhanced FTMW spectroscopy alone, and the 0^+ state would have been thought to be the sole ground state. The cavity-enhanced FTMW measurements, however, were highly beneficial owing to the linear dependence of the line intensity with the dipole moment which have allowed many additional pure rotational lines to be measured. Furthermore, while weak lines of the species were visible by simply expanding the precursor at room temperature in the chamber, significant enhancement, by at least a 10-fold factor, was achieved by applying a 1.2 kV discharge between the electrodes. Signals high enough were obtained to detect ^{13}C isotopologues in natural abundance, and partially deuterated variants were also measured using enriched butadiene precursors. From these measurements and the calculated vibrational motion corrections, a partial semi-experimental structure of *gauche*-butadiene has been derived, with a precise determination of the out-of-plane angle of the species (34 °).[6] Subsequent measurements are currently undergoing to determine a full semi-experimental structure.

We would like to note that arriving at an understanding of this elusive molecule depended critically, but counter-intuitively, on the presence of a spectroscopic perturbation. Without the Coriolis-mediated interaction between the 0^+ and 0^- components of the ground state, there would be no way to extract any information about the tunneling dynamics from the current experiments (since the pure rotational transitions remain within a given tunneling

sublevel). Furthermore, without the disruption of the normal spectral pattern by the perturbation, it is much less likely we would have identified the 0^+ and 0^- states as such, which would have led to misassignments or discarding data as possibly due to impurities, etc. Finally, the discovery and appreciation of this perturbation allowed us to reconcile a long-standing dispute in the literature over the correct interpretation of the structure of this important reactive intermediate.[6]

The work on *gauche*-butadiene is a striking example of the complementary nature and close interplay at work when investigating elusive species: very accurate calculations enabled unambiguous experimental detection of *gauche*-butadiene rotational transitions; as a result, owing to the high sensitivity and resolution of the experiment, the observation of tunneling doublets has been responsible for a deeper theoretical investigation of the potential energy surface of *gauche*-butadiene. Taken together, this joint experimental and theoretical study has established beyond any reasonable doubt that the second conformer of butadiene adopts a *gauche* form in the gas phase.

The results on *gauche*-butadiene have also inspired a subsequent theoretical investigation of the potential energy profile of several heterodienes, as a function of the torsion angle, suggesting the existence of a 1,4 π-interaction[68] as the driving force for the *cis* to *gauche* relaxation, rather than a steric interaction between the inner two terminal hydrogens. The work performed on butadiene can also serve as a template for substituted variants, such as isoprene, for which the *gauche* rotamer is expected to show the same type of tunneling splitting.

3.2 SiCSi

A second example illustrating the power of a joint high-level theoretical and experimental investigation is disilicon carbide, SiCSi. This triatomic molecule has long been known to be a prominent fragment in the vaporization of solid silicon carbide,[69–73] and has been implicated in astrochemical models as a key species,[74,75] along with SiC_2, in the silicon chemistry of certain carbon-rich evolved stars. As with *gauche*-butadiene, early calculations regarding its structure (linear or bent) were fraught with ambiguity but high-level quantum chemical calculations have since settled on a slightly bent structure with C_{2v} symmetry.[76] This simple species, however, proved elusive to rotational spectroscopy, or for that matter nearly any spectroscopic analysis until quite recently. From a theoretical perspective, it has a modest dipole along its *b*-axis ($\sim 1\,\mathrm{D}$),[7] but large amplitude motion and the sensitivity of its rotational spectrum to the quality of the calculations make precise predictions very challenging: for instance, consideration of the zero-point vibrational motion shifts the A rotational constant upwards by 2 GHz compared to the value from considering the equilibrium structure alone. On the experimental side, owing to nuclear spin statistics, it possesses very few low-J, low-frequency rotational transitions. Of crucial importance is the $1_{1\,1} - 2_{0\,2}$ transition which is predicted to lie around 42.7 GHz, just above the nominal high-frequency limit of a standard cavity-enhanced FTMW spectrometer such as ours (at about 40 GHz). Measurements above 40 GHz to perhaps as high as 43 GHz, however, can be made if a line is very strong (e.g., SiO at 43423.8 GHz), but wide searches are rarely feasible.

To overcome this difficulty, the "trick" to detecting SiCSi was to instead target its ^{13}C variant first using samples enriched in ^{13}C, i.e., $^{13}CH_4$. The key feature of Si^{13}CSi is that

its strong $1_{1\,1} - 2_{0\,2}$ transition is shifted down in frequency compared to normal SiCSi by nearly 10 % (42663 vs. 38578 MHz; see Table 4) where wide surveys are readily performed with our cavity-enhanced FTMW instrument. On the basis of predictions at the frozen core-CCSD(T)/PVQZ level of theory, and including vibrational corrections calculated using VPT2, the discharge products of a mixture of SiH_4 and $^{13}CH_4$ were investigated in a 1.5 GHz-wide region around the prediction for the $1_{1\,1} - 2_{0\,2}$ line of Si^{13}CSi (−1 % to +2 % of the predicted frequency, Figure 6). To cover this spectral region with a signal-to-noise ratio (SNR) allowing the confident detection of new transitions, approximately 10 h were needed. In total, roughly 15 transitions are observed on the survey, most of them readily assigned to a vibrational progression of the fundamental rotational transition of SiO, one to Si_3, and four to HSiO. Only one strong transition —the strongest one in that region— was unknown in this survey. This line, at 38578 MHz, lies within about 1 % of the best theoretical prediction for the ^{13}C isotopic variant of SiCSi, is discharge dependent, and was confirmed to be both ^{13}C- and Si-containing (since the removal of any of the precursors yield the disappearance of the line). Confirmation that Si^{13}CSi is the carrier of this line was soon provided by detection of the same line of the ^{29}Si and ^{30}Si isotopic variants in natural abundance at the predicted isotopic shifts.

By scaling the theoretical rotational constants of SiCSi by the ratio Exp./Calc. of those of the ^{13}C variant (see Table 4), it was then possible to make improved predictions for the spectrum of normal SiCSi, and using a mixture of SiH_4 and CH_4, equally strong lines of this species were soon found. As indicated from the close agreement of the scaled rotational constants to those derived for SiCSi (Table 4), scaling reduced the search range by roughly

a factor of 100 relative to the original prediction, meaning that a frequency search of only a few MHz was required to detect lines of SiCSi. Ultimately by correcting the experimental rotational constants of the four isotopic variants for zero-point vibrational motion calculated theoretically, a semi-experimental equilibrium structure was derived in which the bending angle of 114.87 ° was accurately determined.[7]

On the basis of the laboratory measurements, evidence was found for SiCSi almost immediately in the evolved carbon star IRC+10216.[77] Remarkably over 110 lines were assigned throughout the millimeter- and submillimeter-wave band in an existing spectral line survey with a single-dish telescope (IRAM 30 m), as were several lines in a published line survey using the Submillimeter-wave Array (SMA).

3.3 GeC_2

Unlike SiCSi, there is not clear theoretical consensus as to the equilibrium structure of germanium dicarbide GeC_2. Although GeC_2 is known to have a very flat surface of potential along the bending coordinate, calculations have been suggested that it might adopt a T-shaped, L-shaped, or even linear structure (Figure 7).[78–80] When GeC_2 adopts a structure with C_{2v} symmetry, the term T-shaped is used here and elsewhere instead of 'cyclic' to more accurately describe its bonding by analogy to isovalent SiC_2, which has significant ionic-like character in which the C_2^- unit is bound to the silicon atomic ion Si^+ by what could be best described as a non-directional bond.[81] While most calculations predict a very small energy difference between the T- and L-shaped forms, the highest-level calculations[82] slightly fa-

vor the L-shaped structure by about 8 kJ/mol,[80] suggesting that this geometry is likely to serve as the global minimum, with the T-shaped form being a saddle point connecting two equivalent L-shaped forms.

To unambiguously establish the ground state of GeC_2, a broadband spectrum between 8 and 18 GHz was recorded using CP-FTMW spectroscopy in which the laser ablated products of a germanium carbide rod were seeded into a supersonic expansion.[8] A real strength of this approach in the present case is that the fundamental rotational transition of all three conformers falls in this frequency band. If detected, these lines provide a highly reliable diagnostic indicator of the structure, or structures, that GeC_2 adopts in the gas phase, since the rotational pattern of each form differs substantially at the CCSD(T)/cc-pwCVTZ level.[82] Surprisingly, a set of strong features was only observed in the frequency region expected for the T-shaped form (Figure 7). The fairly dense pattern of lines is characteristic of a germanium-bearing species since this element has four isotopologues with comparable natural abundance.

In light of this unexpected experimental result — that GeC_2 adopts a T-shaped structure in its ground state – new theoretical calculations have been performed at the CCSD(T)/cc-pwCVQZ level of theory with all electrons included in the correlation treatment.[8] In contrast to previous work, the T-shaped form is now predicted to be the lowest in energy by the tiniest of margins, 0.02 kJ/mol relative to the L-shaped form. Although this energy difference is too small to draw any definitive conclusions, the trend with increasing size of the basis set suggests that the T-shaped form will continue to be favored, in agreement with experiment.

4 Discussion and Prospects

The examples discussed here are intended to give a flavor of the synergy and ultimately the outcome that is possible when high-level calculations and sensitive experiments are brought to bear to investigate elusive species. As exemplified for GeC_2, even the highest-level calculations should be compared with experiment when possible, since there is no *a priori* guarantee of correctness. Even though the most accurate calculations can predict rotational constants to impressive accuracy, of order 0.01% under the most favorable circumstances, this level is still insufficient to confidently make theory-based assignments of rotational lines in complex mixtures, either in the laboratory or in the interstellar medium. By the same token, even the most sensitive high-resolution experiments greatly benefit from the guidance provided by high-level calculations. Such calculations are not limited solely to rotational constants, but commonly include: dipole moment projections, which are essential to ensure that FTMW searches are performed with the optimal amount of microwave power; estimates of fine and hyperfine structure, which can greatly influence the laboratory search range and the expected line patterns; and centrifugal distortion constants. Since the laboratory data are inherently limited in frequency or J value, it may be difficult to predict the deformation of a newly-found molecule from a small data set. As illustrated here for *gauche*-butadiene, calculations were essential not only in making the original detection but in the subsequent spectroscopic analysis of its many isotopic species.

Ultimately it was possible to generate all three elusive species in very high abundance in our molecule sources. By comparing line intensities to that of a polar molecule (OCS)

at a known concentration, we estimate of order 10^{13} molecules per gas pulse for each. At these abundances it was possible to perform extensive isotopic spectroscopy in natural abundance. The resulting semi-experimental equilibrium structures enable rigorous comparison to equilibrium ones calculated purely from theory. The high abundance also underpins their importance; in the cyclization of small hydrocarbons for *gauche*-butadiene, and as seeds of dust formation for SiCSi. With respect to *gauche*-butadiene specifically, the combined analysis lays a solid foundation for comparative studies of its substituted derivatives such as isoprene, which also exists in two distinct conformers, and may exhibit the same tunneling motion.

As discussed in this review, high level calculations and sensitive experiments are mutually beneficial and proven to be effective for the initial detection of several key elusive species. Countless more species remain elusive so far, a few of them of fundamental importance. Three examples of such species are introduced in the final part of this paper: diazene, cyclopropenium ion, and protonated benzene.

4.1 HNNH

Diazene, or di-imide (N_2H_2), the prototype azo-compound, is a widely used reducing agent for double bonds and a crucial intermediate in the selective hydrogenation of olefins.[83,84] While the ground state *trans*-HNNH rotamer has been extensively characterized (see e.g., Refs[85–87]), the *cis* variant has so far eluded direct observation despite intensive experimental and theoretical investigations.[83,88–90] Interestingly, the *cis* isomer is believed to be the reactant in most of the oxidation reactions involving HNNH.[83] Consequently, there is great

practical utility in unambiguously establishing its existence and determining its structure as a means to refine the transition state structures it adopts in reduction reactions.

Several difficulties have so far prevented experimental characterization of *cis*-HNNH: i) it is very reactive, although it can be synthesized and isolated, with a half-life only on the order of a few minutes at room temperature;[91,92] ii) at room temperature only about 0.3 % of the population is expected to be in the *cis* form since this rotamer lies roughly 20 kJ/mol higher in energy than the *trans*;[89] iii) both rotamers have very similar predicted vibrational spectra in terms of frequencies and intensities, which makes disentangling their infrared spectra very challenging, and the reason why some tentative assignments have been called into question;[83] and iv) while polar, the *cis* rotamer has no low-frequency transitions that originate from low-lying rotational energy levels, making detection by conventional FTMW spectrometers difficult. The only transition that is predicted to fall below 40 GHz involves energy levels lying about 15 cm^{-1} (21 K) above ground. Since the rotational temperature in our jet source is often much colder (< 5 K), these levels are not expected to be well populated.

Despite these challenges, detecting *cis*-HNNH should be feasible. Its fundamental transition is predicted near 300 GHz, meaning that detection at this frequency in a buffer gas cell or with supersonic expansion should be straightforward (although likely tedious), since its dipole moment is about 2.7 D [AE-CCSD(T)/PCVQZ μ_e + FC-(T)/ANO1 vibrational corrections]. Additionally, efforts are currently underway to preferentially synthesize the *cis* rotamer *in situ*; these range from photoisomerization of *trans*-HNNH[90] to thermal release from a stable precursor.[93,94]

4.2 Cyclopropenium ion, $C_3H_2D^+$

The cyclopropenium ion, $C_3H_3^+$, familiar in the laboratory as the mass 39 peak in mass spectrometers,[95,96] is almost certainly present in the interstellar gas, where it is thought to be the main source of cyclic C_3H_2 via dissociative recombination.[97] Owing to its planarity and D_{3h} symmetry, the normal isotopic species possesses no electric dipole moment, and consequently no pure rotational spectrum. Because of the separation between the center of mass and charge upon deuteration, however, its isotopic variant c-$C_3H_2D^+$ (as well as c-$C_3HD_2^+$) is imparted with a sizable dipole moment, of order $0.3 - 0.4$ D. Furthermore, its strong "ortho" fundamental transition ($1_{0,1} - 0_{0,0}$) —conspicuous in c-C_3H_2 at 18.3 GHz— is expected to lie at about 9 GHz, well within the operating frequency range of conventional cavity FT microwave spectrometers such as ours.

c-C_3H_2 is so copiously produced in our spectrometer that it is often possible to detect its doubly-substituted ^{13}C isotopic species in natural abundance under optimized experimental conditions. It is unclear, however, what fraction of this production results from ion-molecule reactions versus other pathways such as carbon insertion into acetylene.[98] As a consequence, there is considerable ambiguity as to the experimental conditions that should be used to search for c-$C_3H_2D^+$, but regardless, a gas sample enriched in D (e.g., either D_2 or HCCH) should be used to enhance the production of this partially deuterated ion. Since protonated derivatives can be detected at the level of 10^{-3}-10^{-4} with respect to the neutral parent,[99] there appears to be adequate sensitivity if ion-molecules pathways dominate. Provided that the spectrum of c-$C_3H_2D^+$ can be measured in the laboratory, this ion would be an excellent candidate for astronomical detection despite its modest dipole moment; many deuterated

variants, including some with multiple D substitutions are readily observed in space.

4.3 Protonated Benzene $C_6H_7^+$

$C_6H_7^+$ is the simplest protonated aromatic hydrocarbon, and a model system for understanding electrophilic aromatic substitution reactions, which are of considerable importance in organic chemistry.[100] Despite its importance, controversy has long surrounded the structure of this cation. Most analyses performed in the condensed phase[101,102] are consistent with a σ-type C_{2v} structure, in which two hydrogen atoms are tightly bound to one carbon atom. At high temperatures (above about 150 K), however, there are indications that all of the protons are equivalent (the so-called π-complex), presumably owing to rapid proton migration around the heavy atom ring skeleton. This controversy appears to have been resolved by Solcá and Dopfer[103] who measured infrared-photodissociation spectra of weakly-bound complexes of $C_6H_7^+$ with Ar in the gas phase. On the basis of the close agreement of the observed spectrum in the C-H stretch region compared to that predicted for various structures, compelling evidence was found for the σ complex.

The C_{2v} structure of protonated benzene imparts a sizable dipole moment, 0.87 D along the a-inertial axis,[104] and a rich spectrum in the centimeter-wave band. Like N_2, CO_2, or cyanogen (NCCN), the parent neutral benzene does not possess a rotational spectrum, so optimization of the experimental conditions are somewhat more challenging, but by no means prohibitive, as evidenced from detection of strong lines of NNH^+ rare gas complexes,[105,106] $HOCO^+$,[107,108] and $HNCCN^+$.[99] Relative to $HOCO^+$, however, detection of $C_6H_7^+$ will be

more difficult in two respects: i) its dipole moment is smaller (vs. 2.7 D[109]), and ii) its rotational partition function is larger (100 vs. 6 at 3 K). Nevertheless, neither factor should preclude detection in the laboratory.

Acknowledgments

We are indebted to a large number of co-workers and collaborators who have been involved in many aspects of the work described here. We are particularly thankful to G. Barney Ellison, Robert W. Field, and Matthew J. Nava for useful discussions. M.C.M. gratefully acknowledges NSF grants AST-1615847, CHE-1566266, and DBI-1555781, and NASA grants NNX13AE59G and 80NSSC18K0396. M.-A. M.-D. acknowledges the support from the Programme National "Physique et Chimie du Milieu Interstellaire" (PCMI) of CNRS/INSU with INC/INP co-funded by CEA and CNES, and from the "Investissements d'Avenir" LabEx PALM (ANR-10-LABX-0039-PALM).

References

[1] C. Pérez, S. Lobsiger, N. A. Seifert, D. P. Zaleski, B. Temelso, G. C. Shields, Z. Kisiel, B. H. Pate, *Chem. Phys. Lett.* **2013**, *571*, 1 – 15.

[2] M.-A. Martin-Drumel, M. C. McCarthy, D. Patterson, B. A. McGuire, K. N. Crabtree, *J. Chem. Phys.* **2016**, *144*, 124202.

[3] B. A. McGuire, *Astrophys. J., Suppl. Ser.* **2018**, *239*, 17.

[4] D. Woon, http://www.astrochymist.org/. `http://www.astrochymist.org/`.

[5] K. N. Crabtree, M.-A. Martin-Drumel, G. G. Brown, S. A. Gaster, T. M. Hall, M. C. McCarthy, *J. Chem. Phys.* **2016**, *144*, 124201.

[6] J. H. Baraban, M.-A. Martin-Drumel, P. B. Changala, S. Eibenberger, M. Nava, D. Patterson, J. F. Stanton, G. B. Ellison, M. C. McCarthy, *Angew. Chem., Int. Ed.* **2018**, *57*, 1821–1825.

[7] M. C. McCarthy, J. H. Baraban, P. B. Changala, J. F. Stanton, M.-A. Martin-Drumel, S. Thorwirth, C. A. Gottlieb, N. J. Reilly, *J. Phys. Chem. Lett.* **2015**, *6*, 2107–2111.

[8] O. Zingsheim, M.-A. Martin-Drumel, S. Thorwirth, S. Schlemmer, C. A. Gottlieb, J. Gauss, M. C. McCarthy, *J. Phys. Chem. Lett.* **2017**, *8*, 3776–3781.

[9] T. J. Balle, W. H. Flygare, *Rev. Sci. Instrum.* **1981**, *52*, 33–45.

[10] S. Kunishige, T. Katori, M. Baba, M. Nakajima, Y. Endo, *J. Chem. Phys.* **2015**, *143*, 244302.

[11] J.-U. Grabow, *Fourier Transform Microwave Spectroscopy Measurement and Instrumentation*, American Cancer Society, **2011**.

[12] U. Andresen, H. Dreizler, J.-U. Grabow, W. Stahl, *Rev. Sci. Instrum.* **1990**, *61*, 3694–3699.

[13] S. Kassi, D. Petitprez, G. Wlodarczak, *J. Mol. Struct.* **2000**, *517-518*, 375 – 386.

[14] J.-U. Grabow, E. S. Palmer, M. C. McCarthy, P. Thaddeus, *Rev. Sci. Instrum.* **2005**, *76*, 093106.

[15] G. G. Brown, B. C. Dian, K. O. Douglass, S. M. Geyer, S. T. Shipman, B. H. Pate, *Rev. Sci. Instrum.* **2008**, *79*, 053103.

[16] J. P. Porterfield, S. Eibenberger, D. Patterson, M. C. McCarthy, *Phys. Chem. Chem. Phys.* **2018**, *20*, 16828–16834.

[17] D. P. Zaleski, L. B. Harding, S. J. Klippenstein, B. Ruscic, K. Prozument, *J. Phys. Chem. Lett.* **2017**, *8*, 6180–6188.

[18] J. L. Neill, B. J. Harris, A. L. Steber, K. O. Douglass, D. F. Plusquellic, B. H. Pate, *Opt. Express* **2013**, *21*, 19743–19749.

[19] B. H. Pate, J. L. Neill, *Segmented chirped-pulse fourier transform spectroscopy*, **2014**, US Patent 8,873,043.

[20] E. Kim, S. Yamamoto, *J. Mol. Spectrosc.* **2003**, *219*, 296 – 304.

[21] D. T. Halfen, L. M. Ziurys in *68th International Symposium on Molecular Spectroscopy*, p. EWH07.

[22] *Z. Naturforsch.* **1980**, *35a*, 392–402.

[23] *Z. Naturforsch.* **1992**, *47a*, 342–352.

[24] E. Alonso, L. Kolesnikova, I. Pena, S. Shipman, B. Tercero, J. Cernicharo, J. Alonso, *J. Mol. Spectrosc.* **2015**, *316*, 84 – 89.

[25] G. B. Park, A. H. Steeves, K. Kuyanov-Prozument, J. L. Neill, R. W. Field, *J. Chem. Phys.* **2011**, *135*, 024202.

[26] A. L. Steber, B. J. Harris, J. L. Neill, B. H. Pate, *J. Mol. Spectrosc.* **2012**, *280*, 3–10.

[27] J.-U. Grabow, S. Mata, J. L. Alonso, I. Pena, S. Blanco, J. C. Lopez, C. Cabezas, *Phys. Chem. Chem. Phys.* **2011**, *13*, 21063–21069.

[28] R. E. Smalley, L. Wharton, D. H. Levy, *Acc. Chem. Res.* **1977**, *10*, 139–145.

[29] M. Sun, D. T. Halfen, J. Min, B. Harris, D. J. Clouthier, L. M. Ziurys, *J. Chem. Phys.* **2010**, *133*, 174301.

[30] D. Patterson, E. Tsikata, J. M. Doyle, *Phys. Chem. Chem. Phys.* **2010**, *12*, 9736–9741.

[31] B. Spaun, P. B. Changala, D. Patterson, B. J. Bjork, O. H. Heckl, J. M. Doyle, J. Ye, *Nature* **2016**, *533*, 517.

[32] D. R. Willey, R. L. Crownover, D. N. Bittner, F. C. De Lucia, *J. Chem. Phys.* **1988**, *89*, 1923–1928.

[33] N. R. Hutzler, H.-I. Lu, J. M. Doyle, *Chem. Rev.* **2012**, *112*, 4803–4827.

[34] J. D. Weinstein, R. Decarvalho, T. Guillet, B. Friedrich, J. Doyle, *Nature* **1998**, *395*, 148–150.

[35] D. Egorov, J. D. Weinstein, D. Patterson, B. Friedrich, J. M. Doyle, *Phys. Rev. A* **2001**, *63*, 030501.

[36] Y. Zhou, D. D. Grimes, T. J. Barnum, D. Patterson, S. L. Coy, E. Klein, J. S. Muenter, R. W. Field, *Chem. Phys. Lett.* **2015**, *640*, 124–136.

[37] J. Piskorski, D. Patterson, S. Eibenberger, J. M. Doyle, *ChemPhysChem* **2014**, *15*, 3800–3804.

[38] D. Patterson, M. Schnell, J. M. Doyle, *Nature* **2013**, *497*, 475.

[39] D. Patterson, J. M. Doyle, *Phys. Chem. Chem. Phys.* **2015**, *17*, 5372–5375.

[40] S. Eibenberger, J. Doyle, D. Patterson, *Phys. Rev. Lett.* **2017**, *118*, 123002.

[41] P. B. Changala, M. L. Weichman, K. F. Lee, M. E. Fermann, J. Ye, *Science* **2019**, *363*, 49–54.

[42] G. K. Drayna, C. Hallas, K. Wang, S. R. Domingos, S. Eibenberger, J. M. Doyle, D. Patterson, *Angew. Chem., Int. Ed.* **2016**, *55*, 4957–4961.

[43] D. Patterson, *Phys. Rev. A* **2018**, *97*, 033403.

[44] M. Joost, M. Nava, W. J. Transue, M.-A. Martin-Drumel, M. C. McCarthy, D. Patterson, C. C. Cummins, *Proc. Natl. Acad. Sci. USA* **2018**.

[45] M. C. McCarthy, W. Chen, M. J. Travers, P. Thaddeus, *Astrophys. J., Suppl. Ser.* **2000**, *129*, 611.

[46] J.-U. Grabow, W. Stahl, H. Dreizler, *Rev. Sci. Instrum.* **1996**, *67*, 4072–4084.

[47] J. P. Porterfield, S. Eibenberger, L. Satterthwaite, M. C. McCarthy, D. Patterson, *Rev. Sci. Instrum.* **2019**, *submitted*.

[48] I. M. Mills in *Molecular Spectroscopy: Modern Research*, K. N. Rao, C. W. Mathews (Eds.), Academic Press, **1972**, chapter 3.2.

[49] C. Puzzarini, M. Heckert, J. Gauss, *J. Chem. Phys.* **2008**, *128*, 194108.

[50] K. Raghavachari, G. W. Trucks, J. A. Pople, M. Head-Gordon, *Chem. Phys. Lett.* **1989**, *157*, 479 – 483.

[51] M. Heckert, M. Kállay, D. P. Tew, W. Klopper, J. Gauss, *J. Chem. Phys.* **2006**, *125*, 044108.

[52] H. Lee, J. H. Baraban, R. W. Field, J. F. Stanton, *J. Phys. Chem. A* **2013**, *117*, 11679–11683.

[53] R. J. McMahon, M. C. McCarthy, C. A. Gottlieb, J. B. Dudek, J. F. Stanton, P. Thaddeus, *Astrophys. J., Lett.* **2003**, *590*, L61.

[54] O. Martinez, K. N. Crabtree, C. A. Gottlieb, J. F. Stanton, M. C. McCarthy, *Angew. Chem., Int. Ed.* **2015**, *54*, 1808–1811.

[55] L. McCaslin, J. Stanton, *Mol. Phys.* **2013**, *111*, 1492–1496.

[56] J. Tennyson, *J. Chem. Phys.* **2016**, *145*, 120901.

[57] P. B. Changala, J. H. Baraban, *J. Chem. Phys.* **2016**, *145*, 174106.

[58] *NITROGEN, Numerical and Iterative Techniques for Rovibronic Energies with General Internal Coordinates, a program written by P. B. Changala. http://www.colorado.edu/nitrogen.*

[59] H. Najib, *Mol. Phys.* **2016**, *114*, 2831–2837.

[60] P. Pulay, W. Meyer, J. E. Boggs, *J. Chem. Phys.* **1978**, *68*, 5077–5085.

[61] N. C. Craig, R. L. Sams, *J. Phys. Chem. A* **2008**, *112*, 12637–12646.

[62] P.-Q. Liao, N.-Y. Huang, W.-X. Zhang, J.-P. Zhang, X.-M. Chen, *Science* **2017**, *356*, 1193–1196.

[63] S. V. Krasnoshchekov, N. C. Craig, P. Boopalachandran, J. Laane, N. F. Stepanov, *J. Phys. Chem. A* **2015**, *119*, 10706–10723.

[64] H. C. Choi, M. Kertesz, S. Dobrin, J. Michl, *Theor. Chem. Acc.* **1999**, *102*, 196–206.

[65] B. R. Arnold, V. Balaji, J. W. Downing, J. G. Radziszewski, J. J. Fisher, J. Michl, *J. Am. Chem. Soc.* **1991**, *113*, 2910–2919.

[66] B. R. Arnold, V. Balaji, J. Michl, *J. Am. Chem. Soc.* **1990**, *112*, 1808–1812.

[67] J. J. Fisher, J. Michl, *J. Am. Chem. Soc.* **1987**, *109*, 1056–1059.

[68] K. B. Wiberg, P. R. Rablen, J. H. Baraban, *J. Org. Chem.* **2018**, *83*, 8473–8482.

[69] J. Drowart, G. De Maria, M. G. Inghram, *J. Chem. Phys.* **1958**, *29*, 1015–1021.

[70] J. Drowart, G. DeMaria, *Thermodynamic study of the binary system carbon-silicon using a mass spectrometer*, J. R. O'Connor, J. Smiltens (Eds.), Pergamon Press, **1960**, pp. 16–23.

[71] G. Verhaegen, F. E. Stafford, J. Jr. Drowart, *J. Chem. Phys.* **1964**, *40*, 1622–1628.

[72] R. W. Schmude, K. A. Gingerich, *J. Phys. Chem. A* **1997**, *101*, 2610–2613.

[73] M. Pellarin, C. Ray, J. Lerme, J. L. Vialle, M. Broyer, X. Blase, P. Keghelian, P. Melinon, A. Perez, *J. Chem. Phys.* **1999**, *110*, 6927–6938.

[74] S. Takano, S. Saito, T. Tsuji, *Publ. Astron. Soc. Japan* **1992**, *44*, 469–480.

[75] Y. Yasuda, T. Kozasa, *Astrophys. J.* **2012**, *745*, 159.

[76] N. J. Reilly, P. B. Changala, J. H. Baraban, D. L. Kokkin, J. F. Stanton, M. C. McCarthy, *J. Chem. Phys.* **2015**, *142*, 231101.

[77] J. Cernicharo, M. C. McCarthy, C. A. Gottlieb, M. Agundez, L. Velilla Prieto, J. H. Baraban, P. B. Changala, M. Guelin, C. Kahane, M. A. Martin-Drumel, N. A. Patel, N. J. Reilly, J. F. Stanton, G. Quintana-Lacaci, S. Thorwirth, K. H. Young, *Astrophys. J., Lett* **2015**, *806*.

[78] R. W. Schmude, K. A. Gingerich, J. E. Kingcade, *J. Phys. Chem.* **1995**, *99*, 15294–15297.

[79] Ş. Katırcıoğlu, *J. Mol. Struct.: THEOCHEM* **2003**, *629*, 295 – 302.

[80] P. Wielgus, S. Roszak, D. Majumdar, J. Leszczynski, *J. Chem. Phys.* **2005**, *123*, 234309.

[81] S. C. Ross, T. J. Butenhoff, E. A. Rohlfing, C. M. Rohlfing, *J. Chem. Phys.* **1994**, *100*, 4110–4126.

[82] L. Sari, K. A. Peterson, Y. Yamaguchi, H. F. Schaefer, *J. Chem. Phys.* **2002**, *117*, 10008–10018.

[83] R. A. Back, *Rev. Chem. Intermed.* **1984**, *5*, 293–323.

[84] S. K. Vidyarthu, C. Willis, R. A. Back, R. M. McKitrick, *J. Am. Chem. Soc.* **1974**, *96*, 7647–7650.

[85] S. N. Foner, R. L. Hudson, *J. Chem. Phys.* **1958**, *28*, 719–720.

[86] N. C. Craig, I. W. Levin, *J. Chem. Phys.* **1979**, *71*, 400–407.

[87] J. Demaison, F. Hegelund, H. Burger, *J. Mol. Struct.* **1997**, *413*, 447–456.

[88] N. Wiberg, G. Fischer, H. Bachhuber, *Angew. Chem., Int. Ed.* **1977**, *16*, 780–781.

[89] R. K. Chaudhuri, K. F. Freed, S. Chattopadhyay, U. S. Mahapatra, *J. Chem. Phys.* **2008**, *128*, 144304.

[90] N. C. Craig, K. J. Appiah, C. E. Miller, M. V. Seiden, J. E. Varley, *J. Mol. Spectrosc.* **2015**, *310*, 3–7.

[91] N. Wiberg, G. Fischer, H. Bachhuber, *Angew. Chem., Int. Ed.* **1972**, *11*, 829.

[92] F. Hegelund, H. Burger, O. Polanz, *J. Mol. Spectrosc.* **1994**, *167*, 1–10.

[93] E. E. Van Tamelen, R. S. Dewey, M. F. Lease, W. H. Pirkle, *J. Am. Chem. Soc.* **1961**, *83*, 4302–4302.

[94] E. J. Corey, W. L. Mock, *J. Am. Chem. Soc.* **1962**, *84*, 685–686.

[95] A. Korth, M. L. Marconi, D. A. Mendis, F. R. Krueger, A. K. Richter, R. P. Lin, D. L. Mitchell, K. A. Anderson, C. W. Carlson, H. Reme, J. A. Sauvaud, C. D'Uston, *Nature* **1989**, *337*, 53–55.

[96] O. Dopfer, D. Roth, J. P. Maier, *Int. J. Mass Spectrom.* **2002**, *218*, 281–297.

[97] D. Talbi in *IAU Symposium*, Vol. 235 of *IAU Symposium*, p. 176.

[98] R. I. Kaiser, C. Ochsenfeld, M. Head-Gordon, Y. T. Lee, A. G. Suits, *Science* **1996**, *274*, 1508–1511.

[99] C. A. Gottlieb, A. J. Apponi, M. C. McCarthy, P. Thaddeus, H. Linnartz, *J. Chem. Phys.* **2000**, *113*, 1910–1915.

[100] G. A. Olah, *Acc. Chem. Res.* **1971**, *4*, 240–248.

[101] G. A. Olah, J. S. Staral, G. Asencio, G. Liang, D. A. Forsyth, G. D. Mateescu, *J. Am. Chem. Soc.* **1978**, 6299–6308.

[102] H.-H. Perkampus, E. Baumgarten, *Angew. Chem., Int. Ed.* **1964**, *3*, 776.

[103] N. Solcá, O. Dopfer, *Angew. Chem., Int. Ed.* **2002**, *41*, 3628–3631.

[104] H.-F. Chen, Y.-J. Wu, *Comput. Theor. Chem.* **2013**, *1006*, 100 –104.

[105] K. Seki, Y. Sumiyoshi, Y. Endo, *J. Chem. Phys.* **2002**, *117*, 9750–9757.

[106] M. McCarthy, P. Thaddeus, *J. Mol. Spectrosc.* **2010**, *263*, 71–77.

[107] M. Bogey, C. Demuynck, J. L. Destombes, *Astron. Astrophys.* **1984**, *138*, L11.

[108] Y. Ohshima, Y. Endo, *Chem. Phys. Lett.* **1996**, *256*, 635–640.

[109] Bizzocchi, L., Lattanzi, V., Laas, J., Spezzano, S., Giuliano, B. M., Prudenzano, D., Endres, C., Sipilä, O., Caselli, P., *Astron. Astrophys.* **2017**, *602*, A34.

[110] M. J. Jones, S. A. Fleming in *Organic Chemistry*, W.W. Norton & Company, **2014**, chapter 13.10.

[111] B. A. McGuire, M.-A. Martin-Drumel, K. L. K. Lee, J. F. Stanton, C. A. Gottlieb, M. C. McCarthy, *Phys. Chem. Chem. Phys.* **2018**, *20*, 13870–13889.

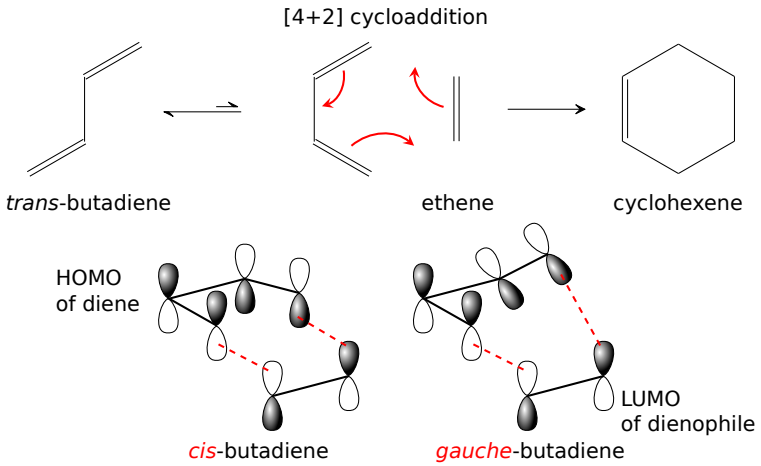

Figure 1: (*top*) Diels-Alder reaction between the simplest diene, butadiene, and the simplest dienophile, ethene, as represented in many chemistry books (e.g., Ref.[110]). (*bottom*) Considerations for orbitals overlap in the Diels-Alder reaction with regard to the *cis* or *gauche* structure of butadiene.

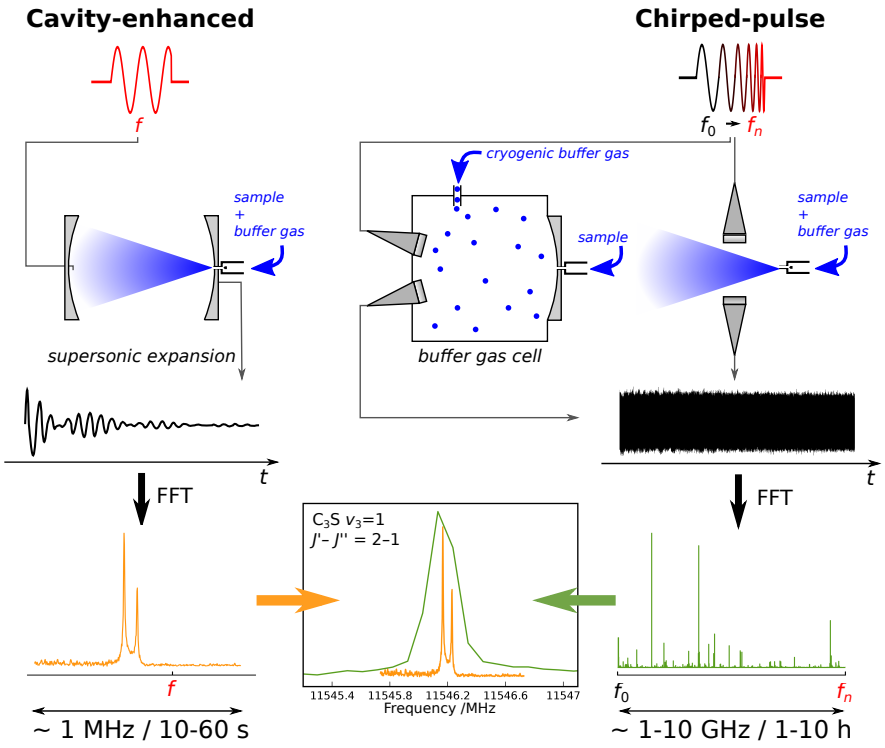

Figure 2: Schematic representation of three different experimental set-ups that can be used in FTMW spectroscopy (see text for details). When the supersonic expansion and the cavity are coaxially aligned in the cavity-enhanced variant, each rotational line consists of a well-resolved Doppler doublet (highlighted in orange). In the broadband variant (here with a IB of 10 GHz), the observed FID is a convolution of FIDs from many different rotational transitions, and the simple, characteristic decay profile, observed on the left-hand part of the figure, is no longer obvious. A comparison of the two line profiles is illustrated for a transition of C_3S recorded with the same supersonic expansion source, and otherwise nearly experimental conditions[111].

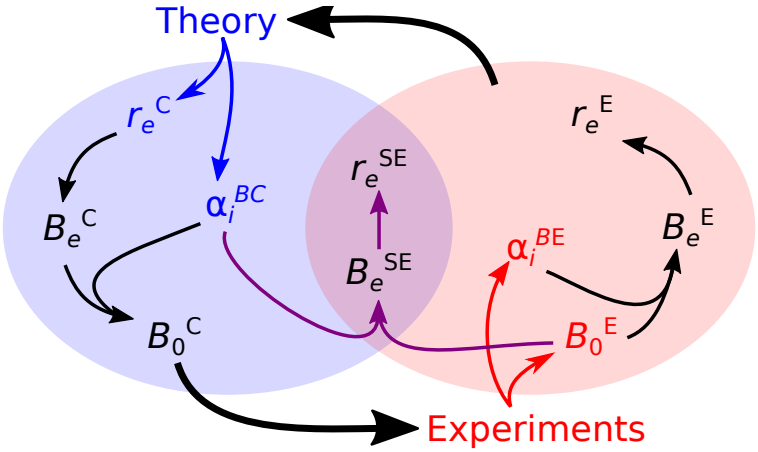

Figure 3: Schematic representation of the interplay between theory and experiment when investigating a new species in the laboratory. The direct output of the calculations (equilibrium structure, r_e^{C}, and vibration-rotation constants, α_i^{BC}) and of the experiment (rotational constants, B_0^{E}, and vibration-rotation constants, α_i^{BE}) are indicated in blue and red, respectively; all the other parameters can be derived from these (see text). C stands for calculated, E for experimental, and SE for semi-experimental, all other notations are described in detail in the text.

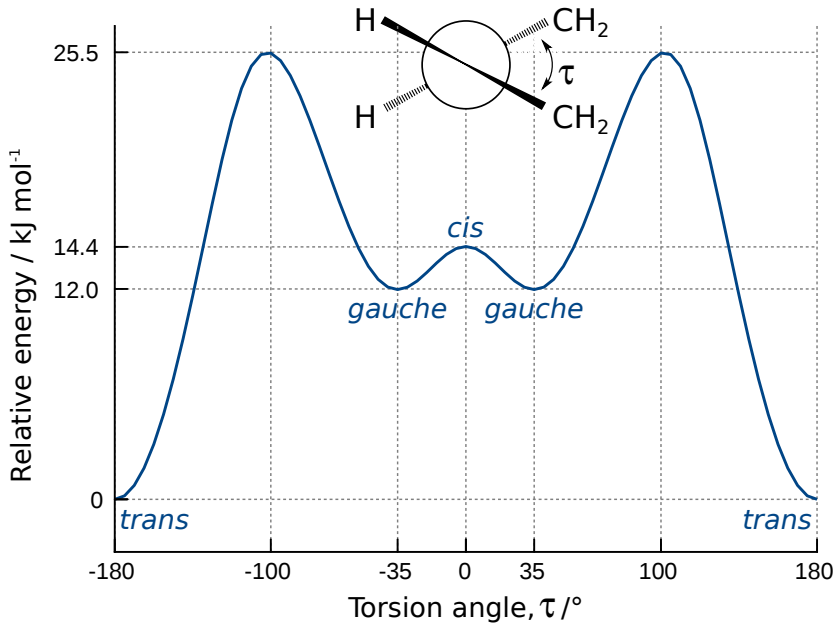

Figure 4: Optimized relative energy of butadiene as a function of the torsion angle from CCSD(T)/ANO1 calculations.

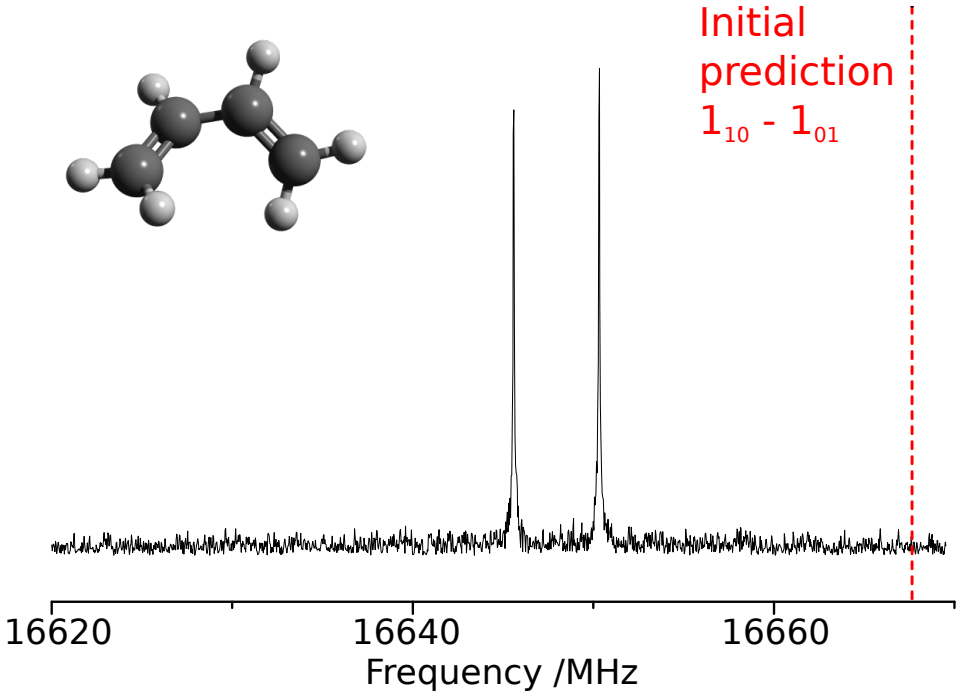

Figure 5: Portion of the CP-FTMW spectrum of butadiene recorded in a buffer gas cell near the theoretical prediction for the $1_{1\,0} - 1_{0\,1}$ transition. Two lines, now assigned to the 0^+ and 0^- components of this transition, are clearly visible within 0.1 % of the prediction.

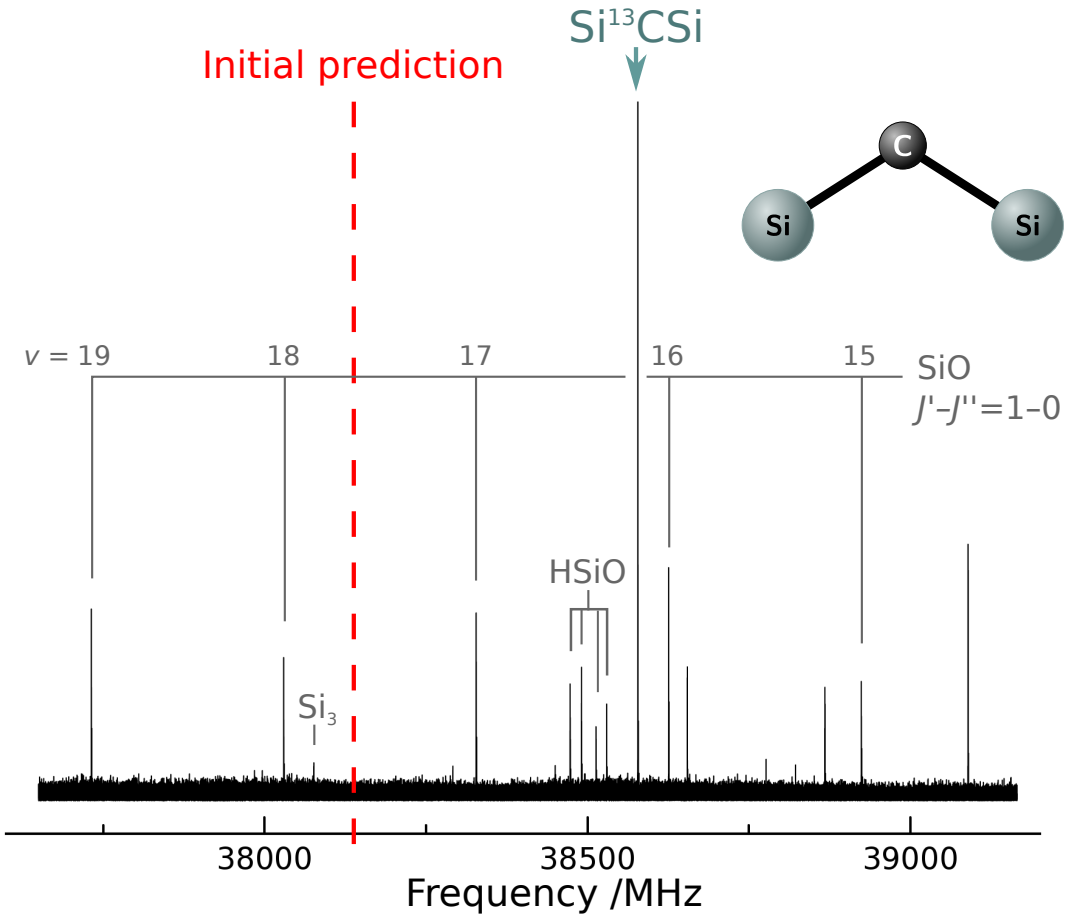

Figure 6: Initial survey around the prediction of $Si^{13}CSi$, starting 2 % higher than the prediction and going down in frequency

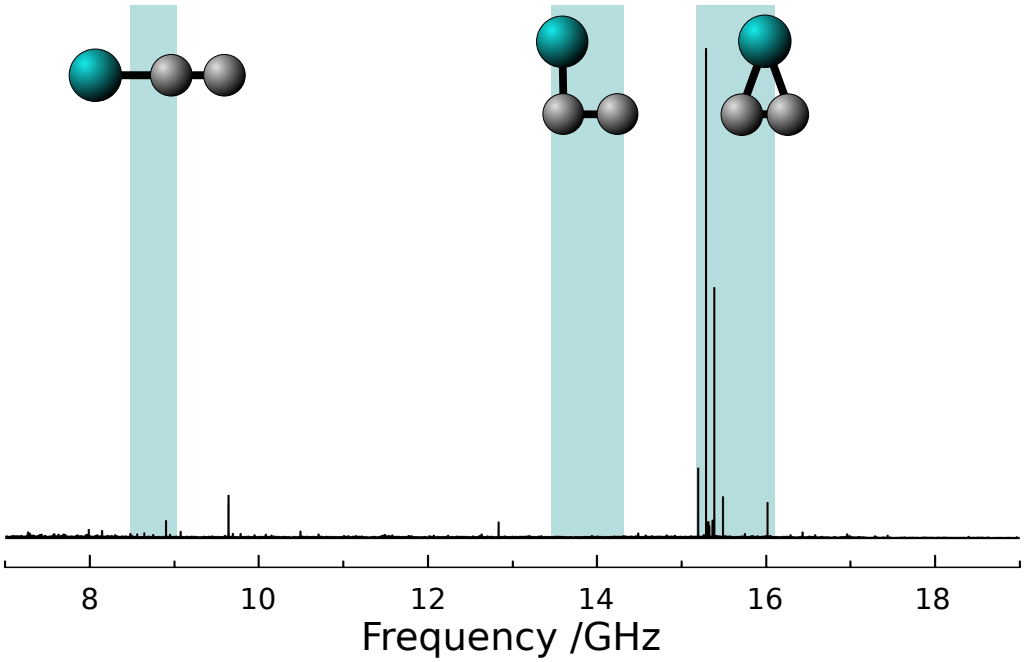

Figure 7: Experimental CP-FTMW spectrum recorded by ablating a germanium carbide rod with 532 nm laser radiation, and expanding the products in a supersonic jet source, after removal of the features from known species. Spectral windows corresponding to a region of ± 3 % about the predicted fundamental transition of linear, L-shapes, and T-shaped GeC_2 are highlighted. Strong features are only visible in the T-shaped region, the remaining lines remain unassigned to date but GeC_2 has been ruled out as a potential carrier.

Table 1: Typical characteristics for three different variants of FTMW spectroscopy in the centimeter-wave band

Parameters	**Cavity-enhanced**	**Segmented**	**Broadband**
IB /MHz	$\sim$1	$\sim$100	$\sim$10,000
Power Density /(mW/MHz)	$\lesssim$1000	$\lesssim$1	$\sim$30
Linewidth /MHz	$\sim$5	$\sim$50	$\sim$50
Dipole moment /D	$\gtrsim 0.1$	$\gtrsim 0.1$	$\gtrsim 0.4$

Table 2: Characteristics for two methods of sample cooling

Characteristics	**Supersonic jet**	**Buffer gas cooling**
Repetition rate /Hz	∼10	∼30,000
T_{rot} /K	2–10	4–10
$T_{vib,el}$ /K	up to 1000s	4–10
Inlet pressure /kTorr	0.5–5	$\gtrsim$0.01
Dilution at inlet /%	99	0
Liquid/solution compatible?	possible	routine

Table 3: Comparison between the experimental and theoretical rotational constants (in MHz) of *gauche*-butadiene. The initial set of theoretical constants enabled the first observation of the molecule while the refined values reproduce the tunneling splitting.

	Exp.	Calc.			
		Initial[a]	δ /%	Refined[b]	δ^c /%
A_0 [d]	21228	21244	-0.08	–	–
B_0 [d]	5670	5654	0.27	–	–
C_0 [d]	4579	4576	0.07	–	–
A_{0^+}	21223	–	–	21219	0.02
B_{0^+}	5671	–	–	5669	0.03
C_{0^+}	4577	–	–	4573	0.09
A_{0^-}	21232	–	–	21226	0.03
B_{0^-}	5667	–	–	5666	0.02
C_{0^-}	4581	–	–	4576	0.11

[a] B_e: AE-CCSD(T)/PCVQZ, $B_e - B_0$: FC-CCSD(T)/ANO0 (VPT2)
[b] B_e: Extrapolation of AE-CCSD(T)/PCV[T-5]Z + $\Delta(Q)$ ANO0, $B_e - B_0$: FC-CCSD(T)/ANO1 (VMP2)
[c] δ = (Exp. − Calc.)/Calc. × 100
[d] Experimental B_0 values are averages of the B_{0^+} and B_{0^-} values for the 0^+ and 0^- states reported in Ref.[6].

Table 4: Ground state rotational constants of $Si^{13}CSi$ and $Si^{12}CSi$ and comparison with the predictions used at the various stages of the experimental search. Consequence on the frequency of chosen transitions of SiCSi: by scaling the rotational constants of the δ obtained for each constant, the prediction for the main species is much more accurate. All values in MHz.

	Exp.	Initial Pred.[a]		Scaled Pred.[b]	
		Value	δ^c /%	Value	δ^c /%
$Si^{13}CSi$					
A_0	59948.0	59257.2	1.2	–	–
B_0	4396.7	4340.9	1.3	–	–
C_0	4084.8	4034.6	1.2	–	–
$f_{1_{1\,1}-2_{0\,2}}$	38578.0	38166.7	1.1	–	–
$Si^{12}CSi$					
A_0	64066.67	63313.3	1.2	64051.4	0.024
B_0	4395.57	4339.9	1.3	4395.7	-0.003
C_0	4102.17	4051.8	1.2	4102.2	-0.001
$f_{1_{1\,1}-2_{0\,2}}$	42663.1	42191.1	1.1	42661.5	0.004

[a] FC-(T)/PVQZ equilibrium + VPT2 zero-point vibrational correction
[b] Scaled Pred. ^{12}C = Initial Pred. $^{12}C \times$ (Exp./Initial Pred.)^{13}C
[c] δ = (Exp. − Calc.)/Calc. × 100